J. Electroanal. Chem., 229 (1987) 191–214
Elsevier Sequoia S.A., Lausanne – Printed in The Netherlands

CLAY MODIFIED ELECTRODES

PART VII. THE ELECTROCHEMICAL BEHAVIOR OF TETRATHIAFULVALENIUM-MONTMORILLONITE MODIFIED ELECTRODES *

MICHAEL T. CARTER and ALLEN J. BARD **

Department of Chemistry, University of Texas, Austin, TX 78712 (U.S.A.)

(Received 13th January 1987)

ABSTRACT

Tetrathiafulvalenium (TTF^+) incorporated into a modifying layer of Texas montmorillonite on a platinum electrode surface shows two kinds of voltammetric responses. These may be attributed to interlamellar TTF^+ (type I) (e.g., in presence of F^- and SO_4^{2-}) and extralamellar TTF^+ (type II) (in the presence of Br^- and I^-). Type I behavior is characteristic of the redox chemistry of $(TTF)_2^{2+}$, while type II behavior reflects formation of non-stoichiometric TTF-halides. Non-electroactive, electronically conductive crystals of $TTFBr_{0.7}$ are produced during cycling in 1.0 *M* NaBr. These promote charge transfer from the substrate platinum electrode to solution species and produce a biconductive clay layer. The electrochemistry of the modified electrode is interpreted in terms of a model for hydrated smectite clays.

INTRODUCTION

This paper describes the electrochemical behavior of a Texas montmorillonite (STx-1) modified electrode into which tetrathiafulvalenium ion (TTF^+) has been incorporated. A biconductive modifying layer is formed, under potential control

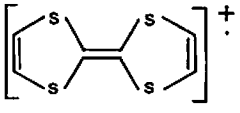

TTF +

* Dedicated to Professor Heinz Gerischer on the occasion of his retirement as Director of the Fritz-Haber Institute.

** To whom correspondence should be addressed.

0022-0728/87/$03.50

and in the presence of bromide, which is similar in properties to that previously described for Nafion–TTF^+ * modified electrodes [1].

An understanding of the electrochemical behavior of intercalated species in clay minerals is of importance because of their use as catalysts in chemical reactions [2,3]. A wide variety of chemical conversions can be carried out at clay surfaces, both directly [4] and via incorporation of catalytic sites [5]. Additionally, sterically and chemically selective heterogeneous catalysts can be produced by pillaring [6]. Stereoselective reactions and resolution of racemic mixtures have also been reported with clays [7,8]. Since clays feature low cost, high thermal stability and resistance to extreme chemical conditions, they represent interesting modifiers of electrode surfaces.

Biconductive phases involve the incorporation of an electronically conductive phase (e.g., a metal or conducting polymer) within an ionically conductive one (e.g., a polyelectrolyte polymer). For example, in an earlier study [1], TTF^+ was incorporated into a layer of Nafion on an electrode surface and by cycling the potential of the electrode in a halide medium, electronically conductive regions and needles of TTF^+-halide were produced. The integration of an ion-exchanging matrix with an electronically conductive structure can result in a more useful modifying layer, because of the enhancement of effective charge transport kinetics toward both bound and dissolved species that is observed with these materials [1b]. A number of inorganic modifying layers have been described [9,10], but biconductive inorganic modifying layers have not been exploited, except for the recent reports on poly(pyrrole)-clay modified electrodes [11].

The modified electrode described here consists of a cation-exchanging matrix of STx-1 with intercalated, electroactive TTF^+. STx-1, a member of the 2 : 1 expanding layer aluminosilicates [12], possesses a high cation-exchange capacity (c.e.c., 84.4 mmol univalent ion/100 g) and a large surface area per unit mass (599 m^2/g) [13] which can allow generation of a high local concentration of electroactive species at the electrode surface. TTF^+, incorporated within the aluminosilicate structure, and in the presence of a suitable electrolyte, forms crystals of non-stoichiometric charge transfer salts [14] whose physical and chemical properties are well characterized. We describe the influence of the clay environment on the formation of the conductive phase and on the general electrochemical behavior of TTF^+.

EXPERIMENTAL

Materials

Tetrathiafulvalene (TTF), 97%, was purchased from Aldrich Chemical Co. and sublimed once before use. Tetrathiafulvalenium chloride (TTFCl) was prepared according to previously reported procedures [1b]. The TFFCl was stored in the dark to avoid decomposition. Fresh, aqueous solutions of TTFCl (1.0 m*M*), for preparation of modified electrodes, were prepared just before each series of experiments.

* Nafion is a trademark of E.I. duPont de Nemours and Co., Inc.,

Solutions were stored in the dark at 4°C under N_2 atmosphere and were discarded after 72 h.

Texas montmorillonite (STx-1) was obtained in the Ca^{2+}-exchanged form from Clay Source Minerals Repository (The University of Missouri, Columbia, MO). The clay was converted to the Na^+ form, purified and freeze-dried according to previously reported procedures [15]. Colloidal suspensions of STx-1 were prepared by mixing the appropriate amounts of freeze-dried clay and water, followed by ultrasonic dispersion for 1 h. Fresh colloidal suspensions were prepared weekly, since the electrochemical behavior of the modified electrode tended to deteriorate with increasing age of the colloid.

Supporting electrolytes (Na_2SO_4, NaF, NaCl, NaI, KCl) were all reagent grade and used without further purification. All solutions were prepared with high purity water (18 MΩ cm) from a Millipore Milli-Q water purification system.

Potassium ferricyanide, $K_3Fe(CN)_6$, was purchased from Aldrich Chemical Co. and used as received. Nafion (1100 eq. wt., 5% w/v in alcohols) was obtained from C.G. Processing, Inc. (Rockland, DE).

Electrode preparation

A platinum disk electrode sealed in glass was used for all voltammetric experiments. The projected area of the disk was 0.017 cm^2, as determined by potential-step chronocoulometry for the reduction of 5.0 m*M* aqueous $K_3Fe(CN)_6$ in 1.0 *M* KCl. The electrode was polished with a slurry of 0.05 μm alumina (Buehler, Lake Bluff, IL) on a felt buffing pad, followed by ultrasonic cleaning for 15 min, prior to each experiment. Periodically, it was also cleaned by fast cycling between +1.30 V and −0.25 V vs. SCE for 1 h in 1.0 *M* H_2SO_4.

STx-1 modified electrodes were prepared by dropping 20 μl of a 0.45 g/l colloidal suspension onto the electrode surface (3.9×10^{-8} mol/cm^2). The solvent was evaporated by gentle heating in air at 46°C. A small tungsten–halogen lamp served as the heat source. Resulting films had a dry thickness of 580 ± 20 nm, as determined with a Sloan Dektak surface profilometer.

Clay-modified electrodes were impregnated with TTF^+ by soaking in 1.0 m*M* aqueous TTFCl for ca. 2 h. The golden color of the resulting film indicated exchange of TTF^+ for Na^+. This electrode is denoted Pt/STx-1/TTF^+. Enhancement of the degree of incorporation of TTF^+ was obtained if the Pt/STx-1 electrode was cycled 15–20 times between +0.2 V and −0.2 V vs. SCE, in the supporting electrolyte of interest prior to immersion in TTFCl solution.

Electrodes for spectroscopic investigations were prepared by spin-coating with a Headway Research model EC-101 photoresist spinner. A known volume (typically 80 μl) of a 2 g/l STx-1 colloidal suspension (in ethanol : water, 50 : 50) was spread onto an optically transparent Sn-doped In_2O_3 (ITO) electrode (Nesatron, PPG Industries). With continuous heating by heat gun, the rotation rate was slowly increased to 1000 rpm until the solution evenly coated the electrode surface (typically 1.0 cm^2). When dry, films had a uniform blue color, indicating a dry film thickness of about 100 nm [16]. Profilometry was not done on these films.

Nafion films were cast on the Pt and ITO substrates for comparison to the behavior of STx-1 films. Typically, 10 μl (Pt) or 50 μl (ITO) of a 1% solution was used. When prepared analogously to the STx-1 films, Nafion films were ca. 300 nm thick on Pt and 100 nm on ITO (by observation of the color of the electrode surface). These electrodes are denoted Pt/Naf/TTF^+ and ITO/Naf/TTF^+, respectively.

Instrumentation

Electrochemical measurements were made with a Princeton Applied Research (PAR) model 173 potentiostat, model 175 universal programmer and model 179 digital coulometer. Current–voltage curves were recorded on a Houston Instruments model 2000 X–Y recorder. Some electrochemical measurements were made using a Bioanalytical Systems model BAS-100 electrochemical analyzer.

An undivided cell, with 20 ml volume was used for all voltammetric measurements with a 1.0 cm^2 Pt flag counter electrode and saturated calomel reference electrode (SCE). Modified electrodes were transferred to the cell, containing only supporting electrolyte, for measurements. The resistance between working and counter electrode of the assembled cell was 145 Ω, as measured with a Yellow Springs Instruments model 35 conductance meter.

Spectroscopic measurements were done on a Hewlett-Packard model 8450A spectrometer. Optical photomicrographs of electrodes were taken with an Olympus model BHTU microscope equipped with an Olympus model PM10-AD photomicrographic system. All experiments were carried out at the ambient temperature of the laboratory (24–26 °C).

RESULTS

Two different voltammetric responses were observed with Pt/STx-1/TTF^+. The first was observed in all of the electrolytes investigated and is designated "type I". The second was observed only after more extended cycling in Br^- and I^- media and is designated "type II". Type II behavior was analogous to that observed previously for TTF^+ in Nafion modifying layers under similar experimental conditions. Potentials and currents are referred to in the text by superscripts (E^{I}_{pc}, E^{II}_{pc}, etc.) to clarify which behavior is being discussed.

Cyclic voltammetry. Type I behavior

Typical type I cyclic voltammetric behavior (CV) is shown in Fig. 1 with 1.0 *M* NaF as supporting electrolyte. Type I behavior featured a single, well-defined and symmetrical cathodic wave on the initial negative-going scan and a nearly identically shaped anodic wave on scan reversal, in the potential range corresponding to $TTF^{+/0}$.

The rate of incorporation of TTF^+ into STx-1 can be obtained, as shown in Fig. 2, by monitoring the cathodic peak current (i^{I}_{pc}) with time of contact with the 1.0

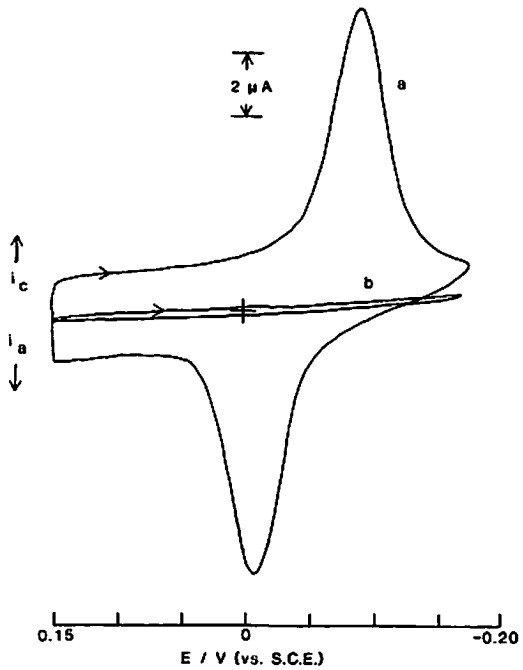

Fig. 1. Cyclic voltammetry of Pt/STx-1, type I behavior (a) in the presence, (b) in the absence of intercalated TTF^+. First cycle at a freshly prepared electrode, c_{TTF^+}, 0.09 *M*. Supporting electrolyte, 1.0 *M* NaF. Sweep rate, 50 mV/s, initiated at +0.15 V vs. SCE.

m*M* TTFCl solution. The supporting electrolyte in this case was 1.0 *M* Na_2SO_4. The magnitude of i^I_{pc} increased linearly with time, up to ca. 2 h and then remained constant. The plateau of Fig. 2 corresponded to a charge equivalent to an amount of TTF^+ 9.5% of that expected based on the c.e.c. of STx-1 of the thickness used,

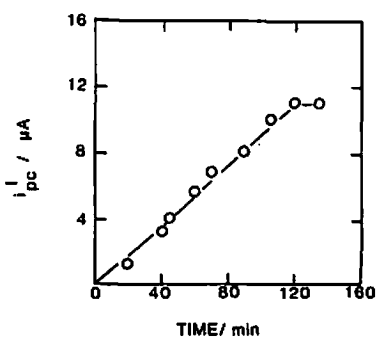

Fig. 2. Dependence of cathodic type I peak current on soaking time in 1.0 m*M* TTFCl. Supporting electrolyte, 1.0 *M* Na_2SO_4. Sweep rate, 50 mV/s.

assuming that all cation-exchange sites were occupied by TTF^+. Maximum loading of the clay films, in terms of electroactive equivalents of TTF^+, was comparable for all electrolytes investigated.

The cathodic peak current increased linearly with sweep rate (v) up to slightly greater than 50 mV/s. Thereafter, a negative deviation was observed, presumably as the overall rate of charge transport in the film became limited by movement of electrolyte ions. For $v \leqslant 50$ mV/s, plots of i_{pc}^{I} vs. v intersected the origin. The apparent diffusion coefficient, D_{app}, for TTF^+ in the clay was estimated from the time (t) required to traverse the entire cathodic CV wave, at $v = 50$ mV/s. When the film has been exhaustively reduced, the effective thickness of the diffusion layer is equal to the thickness of the modifying layer (d). This may be taken as [17]

$$\tilde{d} = (2D_{app}t)^{1/2} \tag{1}$$

From the experimentally determined dry film thickness (580 nm), the average value over all electrolytes studied was $D_{app} = 4.8(\pm 1.4) \times 10^{-10}$ cm^2/s. This should be taken as a lower limit for D_{app}, since some swelling of the film in the supporting electrolyte might occur. The reported value of D_{app} of TTF^+ in Nafion is 8×10^{-7} cm^2/s [1c]. The value estimated by the method described above agreed well with that calculated from the peak current at higher scan rates, assuming a diffusion controlled process [17b]. Values of 6.2×10^{-10} cm^2/s (1.0 M NaCl, $c_{(TTF)_2^{2+}} = 0.03$ M) and 1.0×10^{-10} cm^2/s (1.0 M NaBr, $c_{(TTF)_2^{2+}} = 0.02$ M) were obtained from i_{pc}^{I}–$v^{1/2}$ data obtained at $v \geqslant 100$ mV/s. In this calculation the concentration of TTF^+ was estimated as follows.

Type I behavior displayed typical thin-layer characteristics [18], in the range 5 mV/s $\leqslant v \leqslant$ 50 mV/s. Consequently, the electroactive concentration of TTF^+ could be obtained by

$$Q_c^{I} = nFVc \tag{2}$$

where Q_c^{I} is the charge under the thin-layer cathodic CV wave at 50 mV/s, n is the number of electrons involved, V is the volume of the film based on the electrode area and dry film thickness and c is the film concentration of TTF^+. Calculation of apparent diffusion coefficients for type I behavior, as given above, assumed that the dimer dication, $(TTF)_2^{2+}$, was the predominant film species, with $n = 2$. This assumption is based on UV–visible spectroscopic data (see below). The fraction of the c.e.c. (in terms of moles of TTF^+) represented by F, with $n = 1$, was determined. Typical results are shown in Table 1, under the heading "type I". The electroactive concentration, in all cases, represented less than 10% of that predicted for full ion exchange. Electroactive concentrations in Nafion films are typically 3 times larger than those in clays.

To determine whether or not type I behavior was associated with non-stoichiometric phase formation, a series of supporting electrolytes was investigated, including those which are known to form such phases with TTF^+ (Cl^-, Br^-, I^-) and those which do not (F^-, SO_4^{2-}). The results, summarized in Table 2, indicated only a

TABLE 1

Film concentrations and electroactive fractions from cyclic voltammetry [a]

Type	Medium	Q_a/Q_c	c_0/M	F [b]
I	Na_2SO_4	1.01	0.10	0.096
I	NaF	0.85	0.09	0.086
I	NaCl	1.15	0.08	0.076
I	NaBr	1.18	0.07	0.067
I	NaI	1.06	0.07	0.067
II	NaBr	2.23	0.01	0.01
II	NaI	0.82	0.03	0.03

[a] Determined at $v = 50$ mV/s in 1.0 M supporting electrolyte.
[b] Fraction of the maximum concentration predicted for the clay film, based on the dry film volume and the c.e.c. of STx-1 (1.04 M), assuming $n = 1$ for type I waves and $n = 0.7$ for type II waves.

small effect of the nature of the anion on the peak potentials, E^I_{pc} and E^I_{pa}. Much larger effects would be predicted in the case of formation of a non-stoichiometric TTF-halide [1].

The widths of the CV waves at half-maximum height, $\Delta(E^I_p)_{1/2}$, were narrower than the value of 90.6 mV predicted for a reversible, one electron reaction for a surface confined species [19] and depended on the supporting electrolyte (Table 2). Values of $n > 1$ are suggested by the narrowness of these waves. The splitting between the cathodic and anodic peak potentials, ΔE^I_p, was relatively insensitive to the nature of the supporting electrolyte. Values ranged between 63 and 85 mV, depending on the supporting electrolyte. These values were also larger than expected for a reversible, surface-confined redox couple, where ΔE_p would be zero [19].

Overall, CV waves were better defined in STx-1 for some electrolytes (notably NaF and Na_2SO_4) than in the analogous Nafion experiment. For example, the Nafion experiment corresponding to that shown in Fig. 1 featured only very broad, ill-defined CV waves, due to the sluggishness of ion transport through the film in response to change in electrode potential [20]. Clay films of approximately the same

TABLE 2

Cyclic voltammetry of Pt/STx-1/TTF^+. Type I behavior [a]

Medium [b]	c/M [c]	$-E_{pc}$/V	$-E_{pa}$/V	ΔE_p /mV	$\Delta(E_{pc})_{1/2}$ /mV	$\Delta(E_{pa})_{1/2}$ /mV
Na_2SO_4	0.01	0.093	0.010	83	39	50
NaF	0.09	0.093	0.008	85	47	46
NaCl	0.08	0.108	0.035	73	35	37
NaBr	0.07	0.118	0.033	85	55	38
NaI	0.07	0.130	0.067	63	31	27

[a] $v = 50$ mV/s. All potentials were measured in V vs. SCE.
[b] All electrolytes were 1.0 M.
[c] Electroactive concentrations as given in Table 1.

thickness gave better developed CV waves at the same sweep rate, suggesting that the clay is more permeable to anions. For example, the halides, I^- and Br^-, could be oxidized electrochemically at the Pt substrate, indicating the permeability of the 580 nm clay film to these species.

The CV response described above decayed slowly with time. The rate of loss of the electrode response depended upon the supporting electrolyte used. The waves decayed more rapidly with increasing activity of the electrolyte. This can probably be attributed to slow exchange of the electroactive TTF^+ by Na^+ ions from the supporting electrolytes.

Electrochemical inactivation of neutral TTF on clay

Maintenance of Pt/STx-1/TTF^+ in the reduced form for extended times (either by slow scanning or holding the potential of the electrode at −0.15 V vs. SCE) resulted in loss of electroactivity for the reoxidation of TTF. A typical result is shown in Fig. 3 for the case of 1.0 *M* NaCl electrolyte. The freshly prepared electrode gave the typical type I CV response, as depicted in curve (a) of Fig. 3. After the potential was scanned through the cathodic wave, it was held at the negative limit for 2 min. The subsequent positive-going scan (b) showed a greatly diminished wave for reoxidation of TTF to TTF^+ and continuing the scan with a negative-going sweep showed only a small, ill-defined wave for reduction of TTF^+. The oxidized form could be recovered to the extent of ca. 50% (c) either by holding the potential of the working electrode at +0.15 V vs. SCE or at open circuit for 1–2 min. This cannot be accounted for by leaching of the electroactive material from the film. When the experiment described above was done with removal of the fully reduced electrode from the solution, rinsing and transfer to fresh supporting electrolyte, identical results were obtained. The phenomenon described here occurred on a time scale slower than the voltammetric measurement, because approximately equal amounts of charge were passed for both the cathodic and anodic processes at typical sweep rates (50 mV/s, Table 1). Thus, some process which deters oxidation of TTF occurs. The regeneration of the oxidized form under open-circuit conditions suggests that this phenomenon is internal to the clay–TTF^+ system. The regeneration was not, however, constant with time. If one attempted to regenerate TTF^+ after exhaustive reduction several times at the same electrode, the amount of oxidized form regenerated (as measured by the value of $i^{\mathrm{I}}_{\mathrm{pc}}$) decreased for each new regeneration. Regeneration ceased completely within 2–3 repetitions. This suggests that the sites in the clay which are responsible for this behavior are depleted with time and are not regenerated following oxidation of neutral TTF.

Cyclic voltammetry. Type II behavior

Upon extended cycling in 1.0 *M* NaBr and 1.0 *M* NaI, type I behavior was gradually replaced by a new set of sharp, more widely spaced, redox waves, denoted type II (Figs. 4 and 5). These waves became progressively larger with time and

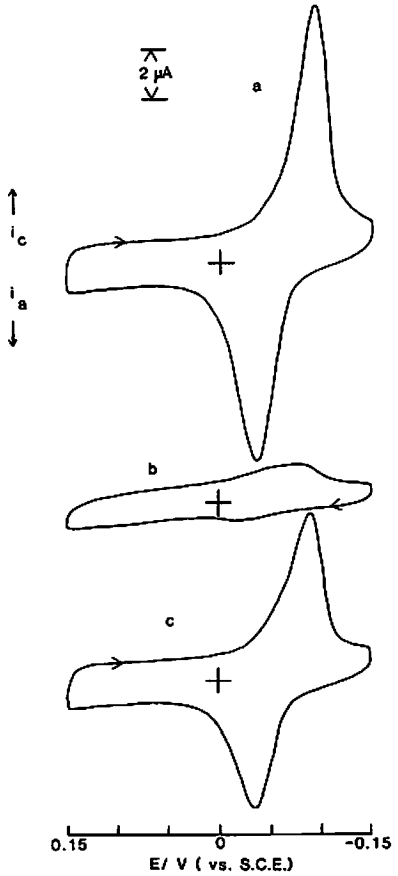

Fig. 3. Loss and recovery of CV response for Pt/STx-1/TTF^+, type I behavior, at (a) freshly prepared electrode, (b) the same electrode as in (a) but following a potential hold at −0.15 V vs. SCE for 2 min and (c) at the same electrode after holding the potential at +0.15 V vs. SCE for 2 min after the procedure in (b). Scans (a) and (c) were initiated at +0.15 V and (b) at −0.15 V. Supporting electrolyte, 1.0 *M* NaCl. Sweep rate, 50 mV/s.

finally reached a steady-state size and shape, which persisted with continuous cycling. This steady-state response disappeared if the film was immersed at open circuit in supporting electrolyte for 12 h. In contrast to type I behavior, no recovery of type II behavior was obtained. This loss of electroactivity was most likely due to leaching of electroactive material from the film over the long term. Type II behavior was not observed at electrolyte concentrations below 1.0 *M*, in contrast to Pt/Naf/TTF^+ [1b], which gave these kinds of waves, with slight distortion in shape at lower supporting electrolyte concentrations.

Typical type II CV results are shown in Fig. 4 for 1.0 *M* NaBr and in Fig. 5 for 1.0 *M* NaI. The voltammetric characteristics for type II behavior in clay (compared

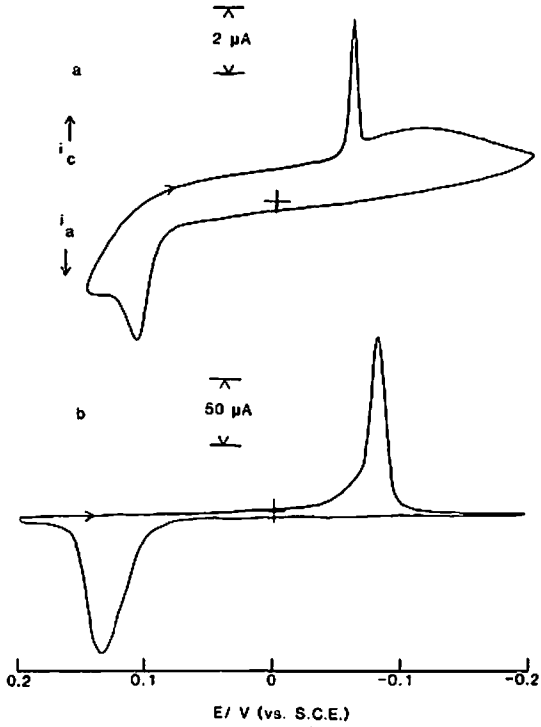

Fig. 4. Cyclic voltammetry of (a) Pt/STx-1/TTF^+, 43rd cycle, steady-state type II behavior. c_{TTF^+}, 0.02 *M* and (b) Pt/Naf/TTF^+, 4th cycle. c_{TTF^+}, 1.2 *M*. Supporting electrolyte, 1.0 *M* NaBr. Sweep rate, 50 mV/s.

to Nafion) are summarized in Table 3. Peak currents increased linearly with v in the intermediate range 5 mV/s $\leqslant v \leqslant$ 50 mV/s, with negative deviations at higher v, as for the type I behavior.

The data shown in Table 3 suggest that the type II process of Pt/STx-1/TTF^+

TABLE 3

Cyclic voltammetry of Pt/STx-1/TTF^+. Type II behavior [a]

Medium	Modifying layer	c/M [b]	E_{pc}/V	E_{pa}/V	ΔE_p/V	$\Delta(E_{pc})_{1/2}$ /mV	$\Delta(E_{pa})_{1/2}$ /mV
NaBr	STx-1	0.02	−0.061	0.110	0.171	7	30
	Nafion	1.2	−0.081	0.134	0.215	15	32
NaI	STx-1	0.06	−0.168	0.055	0.223	18	65
	Nafion	0.35	−0.177	0.027	0.204	13	32

[a] Sweep rate used was 50 mV/s. All potentials were measured with respect to SCE. Supporting electrolytes were 1.0 *M*.

[b] Electroactive concentration of TTF^+ determined as described in Table 1.

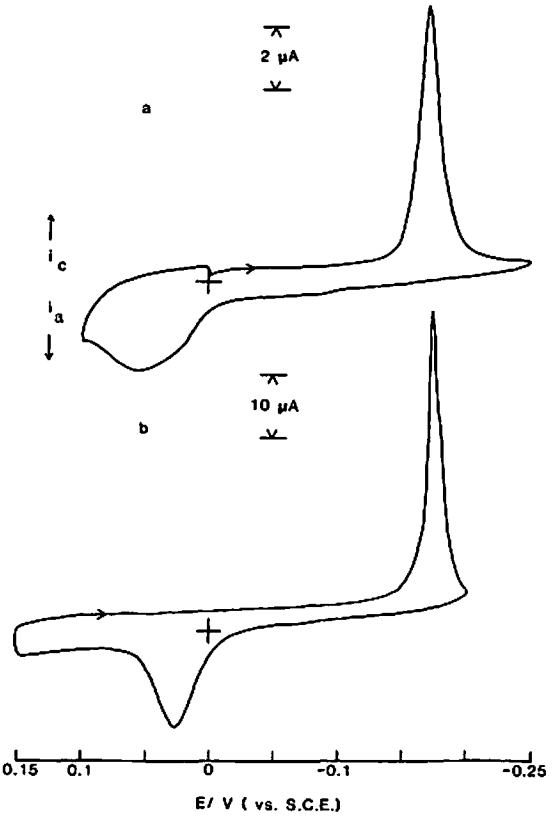

Fig. 5. Cyclic voltammetry of (a) Pt/STx-1/TTF^+, 10th cycle, steady-state type II behavior. c_{TTF^+}, 0.06 *M* and (b) Pt/Naf/TTF^+, 7th cycle. c_{TTF^+}, 0.35 *M*. Supporting electrolyte, 1.0 *M* NaI. Sweep rate, 50 mV/s.

(Figs. 4a and 5a) was quite similar to that of Pt/Naf/TTF^+ (Figs. 4b and 5b), under the same experimental conditions, so that the processes in clay are probably the same as those in Nafion. Type II behavior of Pt/STx-1/TTF^+ featured extremely narrow, sharp cathodic CV waves in both Br^- and I^- media. Scan reversal past the cathodic wave produced a somewhat broader anodic wave for reoxidation. The potentials at which these waves occurred were comparable in STx-1 and Nafion modifying layers (Table 3).

Both the cathodic and anodic waves exhibited hysteresis upon scan reversal part way into the rising portion of the wave. The origin of this effect and the sharpness of the cathodic CV wave have been explained for Pt/Naf/TTF^+ in terms of attractive interactions between the oxidized species [1c]. Values of ΔE_p^{II} were also quite similar to the Nafion case (Table 3), suggesting formation of similar products during electrochemical cycling in the two modifying layers.

Effective diffusion coefficients, calculated from i_{pc}^{II}–$v^{1/2}$ data at $v \geqslant 100$ mV/s

[17b] were 3.7×10^{-8} cm^2/s (1.0 *M* NaBr, $c_{TTF^+} = 0.01$ *M*) and 2.3×10^{-7} cm^2/s (1.0 *M* NaI, $c_{TTF^+} = 0.03$ *M*), based on a concentration estimated as before from the slow scan results and $n = 0.7$ [1]. The larger D_{eff} found with TTF^+ involved in type II behavior indicates more rapid charge transfer through the film under these conditions.

Cyclic voltammetry. Effect of potential scan rate

E^I_{pc} and E^I_{pa} shifted to more negative and more positive values, respectively, with increasing v, for the intermediate range of v investigated. Curves (a) and (b) of Fig. 6 illustrate the behavior obtained in 1.0 *M* NaBr, for E^I_{pc} and E^I_{pa}, respectively. Analogous results were obtained for type I waves in other supporting electrolytes, and are summarized in Table 4. The data suggest kinetic contributions to both the cathodic and anodic processes, possibly in the form of chemical reactions coupled to

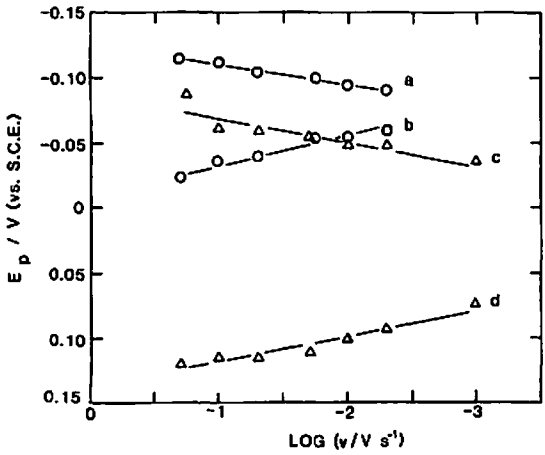

Fig. 6. Dependence of peak potentials on sweep rate for E^I_{pc} (a), E^I_{pa} (b), E^{II}_{pc} (c), and E^{II}_{pa} (d). Supporting electrolyte, 1.0 *M* NaBr. Sweep rates measured in V/s.

TABLE 4

Dependence of peak potentials on sweep rate [a]

Medium	$dE^I_{pc}/d \log v$	$dE^I_{pa}/d \log v$	$dE^{II}_{pc}/d \log v$	$dE^{II}_{pa}/d \log v$
Na_2SO_4	−20	27	–	–
NaCl	−20	19	–	–
NaBr	−15	19	−18	20
NaI	–	–	−13	17

[a] Peak potentials measured in mV vs. SCE. Sweep rates measured in mV/s. All supporting electrolytes were 1.0 *M*.

the electron transfer steps. These shifts are not ascribable to iR drop, which can be estimated to contribute no more than a 2 mV shift in E_p per ten-fold increase in sweep rate, for the larger current magnitudes typically observed in this system (ca. 16 μA).

E_{pc}^{II} and E_{pa}^{II} also shifted to more negative and positive values, respectively, with increasing sweep rate. Figure 6 (curves c and d) illustrate this for 1.0 M NaBr. The dependence of E_{pc}^{II} on log v obtained here was in agreement with that reported for Pt/Naf/TTF^+ (E_{pc}, −19.4 mV/log v) under the same conditions [1c]. Analogous behavior was obtained in 1.0 M NaI (Table 4).

Cyclic voltammetry. Effect of supporting electrolyte concentration

The dependence of E_{pc}^{I} and E_{pa}^{I} on concentration of supporting electrolyte, shown in Fig. 7 for NaBr, suggest that type I behavior was independent of the nature of the halide ion. The behavior of the type I waves in other supporting electrolytes (e.g., Na_2SO_4) were similar to that of Fig. 7. Shifts in E_p^I with concentration of supporting electrolyte were small ($dE_p^I/d \log c$ ca. 1–2 mV). This value is much smaller than that expected for a nernstian process involving Donnan effects [21], e.g.,

$$\sim A^- TTF^+ + e^- + Na^+ \rightleftharpoons \sim A^- Na^+ + TTF \qquad (3)$$

(where $\sim A^-$ represents an anionic site in the clay film) and is consistent with kinetic contributions to E_p^I.

Values of $\Delta(E_{pc}^I)_{1/2}$ and $\Delta(E_{pa}^I)_{1/2}$, however, were affected by supporting electrolyte concentration. Type I waves became narrower, to an appreciable extent,

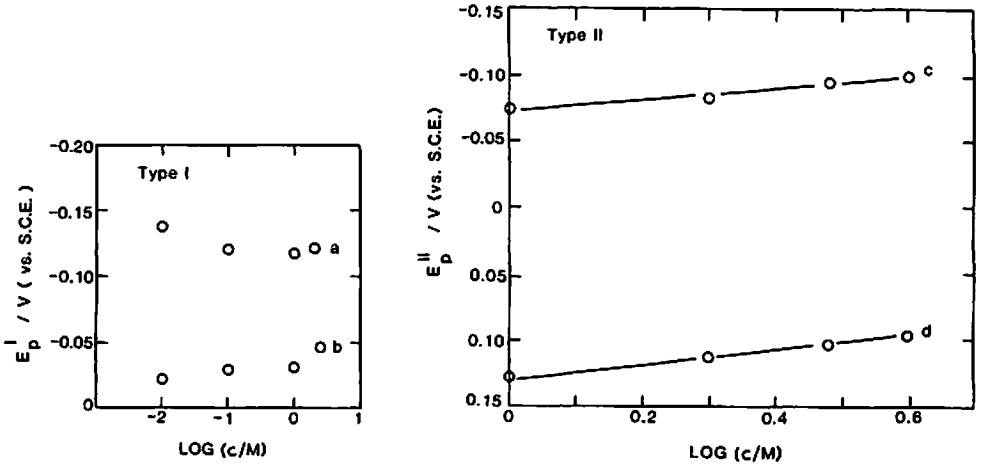

Fig. 7. Dependence of type I and II peak potentials on concentration of supporting electrolyte. Curves (a)–(d) represent E_{pc}^I, E_{pa}^I, E_{pc}^{II} and E_{pa}^{II}, respectively. Supporting electrolyte, NaBr. Concentrations in mol/l. Sweep rate, 50 mV/s.

TABLE 5

Dependence of voltammetric peak widths at half-height for type I waves in NaBr electrolytes [a]

c_{NaBr}/M	$\Delta(E^{I}_{pc})_{1/2}$/mV	$\Delta(E^{I}_{pa})_{1/2}$/mV
0.01	60	76
0.10	60	40
1.0	55	38
2.0	35	35

[a] Measured at 50 mV/s.

with increasing concentration of electrolyte (Table 5). The symmetric, thin-layer shape of the waves was maintained at 50 mV/s, for concentrations of supporting electrolyte of at least 1.0 *M*, with a small amount of diffusional tailing present below this value. The values of $\Delta(E^{I}_{p})_{1/2}$ decreased with increasing concentration of supporting electrolyte. $\Delta(E^{I}_{p})_{1/2}$ was generally influenced in this way, with similar results observed in other media (Na_2SO_4, NaF).

In contrast to type I behavior, type II peak potentials were strongly influenced by supporting electrolyte concentration, as shown in Fig. 7 for NaBr electrolytes. Type II behavior in Pt/STx-1/TTF^+ was not observed at concentrations of Br^- or I^- below 1.0 *M*. The analogous Pt/Naf/TTF^+ experiments showed that, for the Br^- case, the same type of behavior was observed at concentrations of supporting electrolyte as low as 0.1 *M* [1c]. E^{II}_{pc} shifted linearly to more negative potentials by -42 mV and E^{II}_{pa} by -54 mV per ten-fold increase in concentration of NaBr. A similar dependence was found for NaI electrolytes ($dE^{II}_{p}/d \log c$ of -67 and -61 mV for cathodic and anodic waves, respectively). These results are closer to the expected Nernstian shift of -59 mV and suggest that the electron transfer reactions in these processes are coupled to a reaction involving halide.

$$TTF^+X^-_q + q\,e^- \rightleftharpoons TTF + q\,X^- \qquad (4)$$

(where $X^- = Br^-, I^-$). The slightly different slopes obtained in Br^- vs. I^- may be due to different stoichiometries adopted by $TTFBr_q$ and $TTFI_q$ ($0 < q < 1$).

Ultraviolet–visible spectroscopy

To understand better the nature of TTF^+ in the clay environment, the absorption spectra of thin films were investigated. The identification of the absorption bands are based on the reported values of λ_{max} for TTF^0, TTF^+ and $(TTF)^{2+}_2$ in solution [22].

The UV visible spectra of ITO/STx-1/TTF^+ in the oxidized and reduced forms are shown in Fig. 8. The oxidized form of the electrode (Fig. 8a) showed major absorption bands at 380 nm and 520 nm (attributed to intramolecular excitations of $(TTF)^{2+}_2$) and a broad band from 700 to 800 nm (intermolecular charge transfer in $(TTF)^{2+}_2$). A blue shift in the absorbance maximum of TTF^+ from 435 to 380 nm is consistent with dimerization [23]. The reported value of ϵ_{435} for TTF^+ in H_2O,

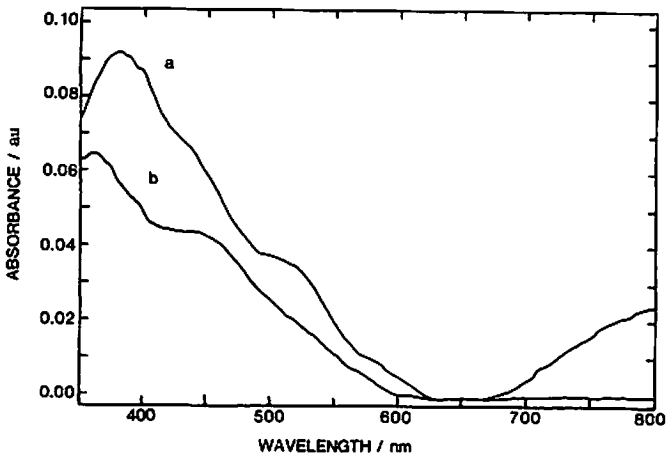

Fig. 8. Electronic absorption spectra of ITO/STx-1/TTF^+ in the (a) oxidized and (b) reduced states.

5.6×10^4 l/mol cm [22c] is four times as large as ϵ_{380} for $(TTF)_2^{2+}$ in ethanol, 1.4×10^4 l/mol cm [22b]. The shoulder at 435 nm for TTF^+ suggests that some monomer may be present in the oxidized film. The spectrum of ITO/STx-1/TTF^+ in the oxidized form was quite similar to that of ITO/Naf/TTF^+, where $(TTF)_2^{2+}$ has been suggested to be the predominant species [1c]. Reduction of the film, by scanning the potential to −0.20 V vs. SCE (in 1.0 *M* NaF) gave the spectrum shown in Fig. 8b. The total concentration of TTF^+ in the oxidized film, based on the dry film thickness and the reported extinction coefficients of TTF^+ and $(TTF)_2^{2+}$, given above, was 1.4 *M*. This corresponded to 10% of that predicted based on the c.e.c. of STx-1, for a fully exchanged film. Following reduction, the spectrum was essentially that of neutral TTF, with $\lambda_{max} = 360$ nm and a smaller, broader band at about 450 nm [22d]. These results suggest that, at the maximum degree of loading, only a fraction of the c.e.c. is exchanged (ca. 10%) and that all of these sites are electroactive.

Optical photomicrography

A portion of a typical surface of the Pt/STx-1/TTF^+ electrode, following extensive cycling in 1.0 *M* NaBr, is shown in Fig. 9. Purple crystals were dispersed over the entire surface of the electrode, many of which had small needles emanating from them. These crystals did not form spontaneously when the electrode was immersed in 1.0 *M* NaBr and not cycled. In contrast, the crystals which have been reported to form within the Nafion/TTF^+ film [1b] can form both spontaneously due to reaction of TTF^+ and Br^- at the Nafion/solution interface as well as with cycling [24]. These crystals are probably conductive, non-stoichiometric $TTFBr_{0.7}$ [1]. The crystals formed within the STx-1 matrix have a considerably different morphology from those formed in Nafion, where long, needle-like structures pre-

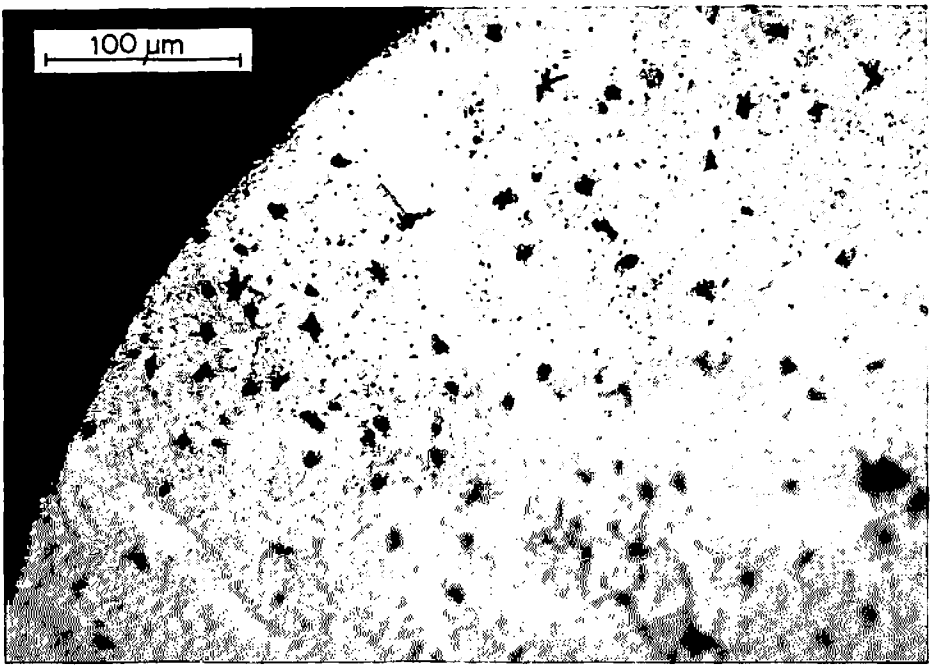

Fig. 9. Optical photomicrograph of Pt/STx-1/$TTFBr_{0.7}$ following extensive cycling in 1.0 *M* NaBr.

dominate [1b]. Thus, the morphology of the conductive phase generated electrochemically depends strongly upon the structure of the environment in which they form.

Mediated electron transfer to solution species

Preliminary experiments suggest that the Pt/STx-1/TTF^+ electrode can mediate electron transfer from the metallic substrate to solution species which are not able to penetrate the clay film. For example, CV of 1.0 m*M* $K_3Fe(CN)_6$ in 1.0 *M* KCl gave the behavior shown in Fig. 10(a), for the bare Pt disk. When the electrode was coated with 1.2×10^{-7} mol univalent ion/cm^2 STx-1, it was rendered much less permeable to $Fe(CN)_6^{3-}$, as shown in curve (b). A significant increase in current for $Fe(CN)_6^{3-}$ was observed, however, following impregnation of the STx-1 film with TTF^+ and growth of $TTFBr_{0.7}$ in 1.0 *M* NaBr (c). The peak current for reduction of $Fe(CN)_6^{3-}$ under these conditions was 57% of that at the bare electrode but 3.7 times greater than at the clay coated electrode in the absence of $TTFBr_{0.7}$. The waves of the $Fe(CN)_6^{3-/4-}$ couple were superimposed upon those of $TTF^{2+/+}$, located at about +0.5 V vs. SCE. The blank experiment shown in curve (d), in which the electrode was prepared identically to that shown in (c), except that TTF^+ was not incorporated into the film (1.0 m*M* NaBr was used in place of 1.0 m*M*

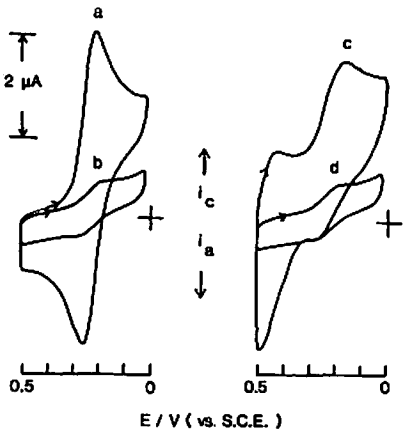

Fig. 10. Mediation of electron transfer to dissolved $K_3Fe(CN)_6$. CV of 1.0 m*M* $Fe(CN)_6^{3-/4-}$ at (a) bare Pt electrode, (b) same electrode as in (a) after coverage by 1.2×10^{-7} mol univalent ion/cm^2 STx-1, (c) after growth of $TTFBr_{0.7}$, and (d) PT/STx-1 without $TTFBr_{0.7}$ but otherwise treated identically to (c). Supporting electrolyte, 1.0 *M* KCl. Sweep rate, 100 mV/s.

TTFCl for the ion-exchange step, as described in the experimental section) showed identical behavior to (b), suggesting that $Fe(CN)_6^{3-/4-}$ electrochemistry occurred at $TTFBr_{0.7}$ and not via diffusion through the clay layer to the Pt substrate.

DISCUSSION

Type I behavior

Incorporation of TTF^+ into STx-1 probably proceeds through intercalation of monomer from 1.0 m*M* TTFCl. When the local concentration of TTF^+ becomes sufficiently high, dimerization to $(TTF)_2^{2+}$ proceeds. This may be represented as

$$A^-Na^+ + TTF^+ \rightarrow A^-TTF^+ + Na^+ \quad (5)$$

$$A^-Na^+ + A^-TTF^+ + TTF^+ \rightarrow A_2^{2-}(TTF)_2^{2+} + Na^+ \quad (6)$$

where A^- represents the fixed ion exchange sites of the aluminosilicate sheet. Dimerization of the planar radical cation TTF^+, on the montmorillonite surface at high concentrations is consistent with the observed absorption spectrum of the modified electrode and with previous observations on TTF^+ [25a] and methylene blue [25b,c], adsorbed on clay surfaces.

The small value for D_{app} for interlamellar $(TTF)_2^{2+}$ suggests that it is strongly associated with the aluminosilicate sheet. Reported diffusion coefficients of tris(2,2′-bipyridyl) metal complexes in clays [15,26] are at least one to two orders of magnitude smaller (10^{-11}–10^{-12} cm^2/s), whereas D_{app} for TTF^+ in Nafion is three orders of magnitude larger [1a]. TTF^+ is more free to diffuse within the clay matrix

than the bulkier metal complexes due to its smaller size, but less so than in Nafion, which is a much less rigid, more fluid-like environment than montmorillonite. The relatively small diffusion coefficient of $(TTF)_2^{2+}$ in montmorillonite reflects the way in which it intercalates into the interlayer region of the aluminosilicate. TTF^+ has been reported to adopt an orientation in which the plane of the sulfur atoms is perpendicular to the aluminosilicate sheet, with partial insertion ("keying") of the TTF^+ hydrogens into the oxide surface [27], in the same manner as found in benzidine/vermiculite intercalates [28]. The keying phenomenon [3b] accounts for the difference in diffusion coefficients noted above. Bulky species with hydrogens available for keying are held rigidly in place. Smaller species may diffuse more rapidly, but the placement of the TTF^+ hydrogens is such that a certain amount of keying takes place. No similar type of association is available in polymer films, and so TTF^+ exhibits much faster diffusion in this medium.

Interlamellar TTF^+ is stabilized significantly with respect to TTF^+ in solution. Inspection of the peak potentials of Table 2, shows that reduction of TTF^+ is shifted to more negative potentials by ca. 400 mV with respect to previously reported potentials for reduction of TTF^+ and its derivatives in solution [29]. The Donnan potential, present at the interface of the bulk supporting electrolyte and the modifying clay layer, may be responsible for the apparent shifts in formal potentials of $TTF^{+/0}$. Donnan equilibria have been implicated recently in the shifts in formal potentials observed for a variety of electroactive metal complexes, incorporated in the polyelectrolyte Nafion, from their values at bare electrodes [21]. Dimerization is also likely to influence the potential shift, since $E^{\circ\prime}$ for non-dimerizing species such as $Ru(bpy)^{2+/3+}$ (bpy = 2,2′-bipyridine) are generally shifted to more positive values when incorporated into clays [30]. The $MV^{2+/+}$ couple (MV = methyl viologen) shows an $E^{\circ\prime}$ essentially unaffected by the aluminosilicate environment [31]. The similarity of the electronic absorption spectra of $(TTF)_2^{2+}$ in solution and that of solid $TTFBr_{0.79}$ [22b] suggests that the interaction of TTF^+ units are similar in these two systems. The charge transfer salts are known to be stabilized toward reduction vs. TTF^+ in solution [1]. Thus, interaction of neighboring TTF^+ molecules in the dimer would be expected to stabilize it in much the same way.

Participation of halide in type I electrochemistry is only possible if the anion can penetrate the zone in which the redox reactions occur. For the interlamellar zone, halide would have to intercalate as a neutral salt [32], because the anionic charges on the aluminosilicate preclude penetration by anions. Ion pairing is negligible at the electrolyte concentrations studied here. The insensitivity of the type I behavior to the nature or concentration of the supporting electrolyte indicates that it has its origin in an anion-inaccessible zone and can therefore be attributed to interlamellar $(TTF)_2^{2+}$.

Values of ΔE_p which deviate significantly from the theoretical value ($\Delta E_p = 0$) for reversible, thin-layer electron transfer have been reported for several systems [33]. Large ΔE_p values are sometimes attributed to slow heterogeneous electron transfer kinetics or film or solution resistance. The symmetrical shape of the type I waves and the low measured cell resistance (145 Ω) rule out resistive contributions.

If one assumes that slow heterogeneous electron transfer kinetics are the cause, one can estimate from the CV response, the heterogeneous electron transfer rate constant, k°, for a surface confined couple by [34]

$$\log k^\circ = -4.24\,\Delta E_p + \log(\upsilon VF/2ART) \tag{7}$$

where ΔE_p is the peak potential separation, $|E_{pc} - E_{pa}|$, in V, υ is the sweep rate in V/s, V is the volume of the thin layer in cm^3, A is the electrode area in cm^2 and F/RT is 38.92 V^{-1} (25 °C). Application of eqn. (7) to the data of Table 2 yields an average value of $k^\circ = 2.6(\pm 0.5) \times 10^{-5}$ cm/s. This should only be taken as approximate since eqn. (7) does not strictly apply for $k^\circ > 10^{-5}$ cm/s [18]. $TTF^{+/0}$ in solution typically shows reversible CV behavior [22a,29], corresponding to $k^\circ > 10^{-3}$ cm/s. The values calculated via eqn. (7) seem to be unreasonably small for the modified electrode. The undistorted shape of the CV waves of the modified electrode support the proposition that the observed ΔE_p^l values are not due to slow electron transfer.

A more reasonable explanation for the observed behavior is that $(TTF)_2^{2+}$ is involved in a square reaction scheme [33], in which the reduced form, generated on the initial negative-going scan, undergoes a subsequent chemical transformation to produce a new reduced form with $E^{\circ\prime}$ different from that of the initial reduced form. Modified electrodes produced by incorporation of electroactive species into electroinactive films, such as Nafion/$Ru(bpy)_3^{2+/3+}$ [35] and Nafion/TTF^+ [1], as well as electroactive polymer coatings, such as poly(vinylferrocene/ferrocinium) [33] exhibit such reaction schemes. Structural changes in a thin film upon oxidation or reduction [36], fast chemical reactions coupled to electron transfer [1c,33,37] and variation in the interactions between electroactive species in the oxidized and reduced forms [38] can contribute to observation of a non-zero ΔE_p.

The small values of $\Delta(E_p^l)_{1/2}$ for interlamellar TTF^+ also suggest interaction of TTF^+ within the film. For the reversible reduction of an oxidized form followed by a first order irreversible decay of the reduced form to some product, the value of $\Delta(E_{pc})_{1/2}$ is predicted to be $66/n$ mV (25 °C) for a scan rate where the rate of the following chemical reaction (described by the first order rate constant, k) is fast compared to υ [39a]. Given that the widths of the CV waves in this study are influenced by the supporting electrolyte concentration (Table 5), the data generally suggest that $n = 2$ (especially for higher NaBr concentrations) for type I cathodic branch, and that the initial oxidized form of the film is $(TTF)_2^{2+}$.

The value of $\Delta(E_{pa})_{1/2}$ for the reversible oxidation of an initially reduced form, followed by irreversible dimerization of the oxidized form is predicted to be $47/n$ mV (25 °C) in the range of υ where the rate of dimerization is fast compared to υ [39b]. The values of $\Delta(E_{pa}^l)_{1/2}$ found here are in agreement with $n = 1$ for 1.0 M Na_2SO_4 and 1.0 M NaF, but are somewhat narrowed ($n > 1$) with respect to this value for the other electrolytes of Table 2. It is possible that the rate of dimerization is affected by the electrolyte activity, because Na^+ must move in and out of the film upon oxidation and reduction (vide infra). An added narrowing of the anodic type I wave could be due to the higher activity of the 1.0 M NaBr and 1.0 M NaI

electrolytes. Increases in electrolyte activity within a film have been reported to affect CV waves of $TTF^{2+/+}$ in poly(phenoxytetrathiafulvalene) thin films in exactly this manner [40].

The sweep rate dependencies of E^{1}_{pc} and E^{1}_{pa} generally corroborate the other evidence, suggesting irreversible chemical steps coupled to the electron transfers [33]. However, the voltammetric criteria for E_RC_1 reactions [39], for the reactions discussed above, requires invoking unreasonably large values of n to fit the data for the slopes of the E_p–log v curves. The actual process in type I behavior may be more complex than the above analysis of the half-heights of the waves suggests.

When the Pt/STx-1/TTF^+ electrode is maintained in the reduced form for long times, TTF^+ is not immediately regenerated during a subsequent positive-going sweep. This suggests that the reduced form may undergo a slow irreversible electroinactivation at the aluminosilicate surface. A similar phenomenon has been reported for $(MV)_2^{2+}$ produced following the reduction of MV^{2+} to MV^+ [31]. In contrast to the MV^{2+}/STx-1 system, where a large fraction (80–83%) of MV^{2+} is rendered electroinactive due to the strong adsorption capacity (SAC) of STx-1 toward MV^{2+} [41], the TTF^+/STx-1 system shows essentially 100% electroactivity, with only a fraction (10%) of the exchange sites of STx-1 occupied by TTF^+. This is likely to be an effect of the ion-exchange equilibrium for TTF^+ and Na^+ between the bulk exchange solution (1.0 m*M* TTFCl) and the clay layer, under the experimental conditions employed here. Regeneration of $(TTF)_2^{2+}$ following electroinactivation at open circuit suggests that regeneration of the oxidized form is accomplished by redox sites within the clay [27,42], probably Fe(II) isomorphously substituted into the aluminosilicate or present as an impurity. The effect of these sites on the electrochemistry of species within clay films has been noted previously [4c,15,43]. Regeneration of $(TTF)_2^{2+}$ can only be accomplished 2–3 times in one film, with decreasing recovery each time, suggesting a sacrificial regeneration mechanism.

The type I electrochemistry is summarized in Scheme 1.

SCHEME 1

$$A_2^{2-}(TTF)_2^{2+} + 2\,Na^+ + 2\,e^- \rightleftarrows 2\,A^-Na^+ + (TTF)_2 \qquad E_1^{\circ\prime}$$

$$\uparrow \qquad\qquad \downarrow$$

$$2\,A^-TTF^+ + 2\,Na^+ + 2\,e^- \rightleftarrows 2\,A^-Na^+ + 2\,TTF \qquad E_2^{\circ\prime}$$

TTF in the clay film is initially in the form of dimer dication, $(TTF)_2^{2+}$. Exhaustive reduction of the film generates an unstable species, $(TTF)_2$, which rapidly decays to monomeric TTF. Reoxidation of TTF produces TTF^+, which then rapidly dimerizes to reform $(TTF)_2^{2+}$. The cathodic branch proceeds at potentials characteristic of $(TTF)_2^{2+/0}$ and the anodic branch at potentials characteristic of $TTF^{+/0}$. The predominant forms of TTF in the film are $(TTF)_2^{2+}$ (oxidized form) and TTF

(reduced form). The separation of peak potentials is therefore a reflection of the stabilization of $(TTF)_2^{2+}$ relative to TTF^+ toward reduction and probably also reflects a structural change in the organization of the electroactive species in the film due to the difference in attractive interactions between TTF^+ and TTF^+ vs. TTF with TTF [38]. The entire redox couple is shifted to more negative potentials vs. solution via the Donnan effect.

Type II behavior

The type II electrochemistry may be treated by analogy to that of the Pt/Naf/TTF^+ electrode [1] and to the electrochemistry of TTF^+ in the presence of halides, reported in other systems [44].

E_{pc}^{II} and E_{pa}^{II} occur at potentials very close to those of Pt/Naf/TTF^+ under the same conditions. The values of ΔE_p and $\Delta(E_p)_{1/2}$ are also comparable in the two cases. The sharpness of the cathodic CV wave and hysteresis in CV upon scan reversal have been explained in terms of phase formation involving TTF^+ and halide ion in the case of Nafion modifying layers. The attractive forces between TTF molecules in the charge transfer salt must be overcome on reduction and give rise to the extremely narrow waves and the hysteresis effect.

These reactions must occur in a halide-accessible zone as indicated by the significant dependencies observed of the voltammetric characteristics on the nature and concentration of the supporting electrolyte. Type II behavior most likely arises from extralamellar TTF^+ (see below). Closely analogous behavior of Pt/STx-1/TTF^+ and Pt/Naf/TTF^+, in Br^- medium, suggest that the same conductive phase is formed in both systems [45a–c]. The behavior in I^- medium also suggests formation of a TTFI charge transfer salt [45d].Type II electrochemistry (Br^- case) is given in Scheme 2, where (ec) and (st) are the eclipsed and staggered conformations, respectively, of TTF molecules in the segregated stacks of the charge transfer salt [1c]. The stable forms of TTF are (ec)$TTFBr_{0.7}$ and (st)TTF. After extended cycling, enough halide is able to penetrate the film to give the electrochemical behavior characteristic of these materials.

SCHEME 2

$$\begin{array}{lll} (ec)TTFBr_{0.7} + 0.7\,e^- \rightleftarrows (ec)TTF + 0.7\,Br^- & & E_1^{\circ\prime} \\ \uparrow \qquad\qquad\qquad\qquad\qquad\qquad \downarrow & & \\ (st)TTFBr_{0.7} + 0.7\,e^- \rightleftarrows (st)TTF + 0.7\,Br^- & & E_2^{\circ\prime} \end{array}$$

Model of the aluminosilicate

The last point to address is the origin of the two voltammetric responses. The structural model upon which the following argument is based is illustrated schemati-

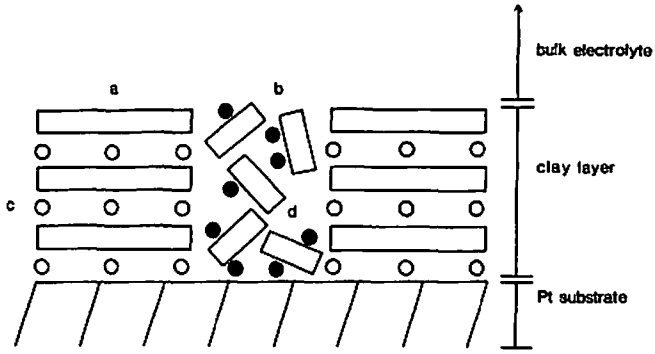

Fig. 11. Schematic representation of Pt/STx-1/TTF^+. Elementary STx-1 platelets are segregated into (a) ordered zones of large, parallel platelets and (b) disordered zones of smaller size particles. $(TTF)_2^{2+}$ may reside as (c) intercalated form in ordered zones or (d) adsorbed to platelet faces in disordered zones.

cally in Fig. 11, which shows the first few layers of clay platelets in the vicinity of the substrate electrode surface. The microstructure of montmorillonite films has been discussed by Cebula et al. [46]. The majority of the elementary clay platelets in films cast on flat substrates (ca. 90%) are oriented parallel to the substrate surface. Oriented domains are composed mainly of larger particles. Smaller particles (the remaining 10%) tend to create stacking defect zones, in which the platelets are more or less randomly oriented. Edge-to-face stacking in the presence of high electrolyte concentrations [12b] and curling of platelet edges [47] probably promote formation of stacking defects.

$(TTF)_2^{2+}$ on outer faces of platelet stacks and in defect zones should be more accessible by halide than $(TTF)_2^{2+}$ intercalated into the parallel stacks of larger platelets. Coulombic repulsion between halide and the anionic charge on the parallel platelets precludes penetration of this region by halide. Extralamellar $(TTF)_2^{2+}$ therefore undergoes electrochemical reaction characteristic of TTF-halides, while interlamellar $(TTF)_2^{2+}$ undergoes electrochemistry characteristic of a halide-independent reaction.

CONCLUSIONS

The presence of defect zones in the structure of montmorillonite films on electrodes is observed for films impregnated with TTF^+. The ability of TTF^+ to participate in separate reaction sequences with and without halide ion allows the defect structure of the clay to be detected electrochemically. The physical differences in the environments of the interlamellar zone and the defect zone are reflected in the diffusion coefficients for the two voltammetric responses of TTF^+.

Biconductive modified electrodes can be produced by the formation of $TTFBr_{0.7}$ within the ion-exchanging montmorillonite matrix. These conductive organic crystals can mediate the transfer of electrons to bulk solution species which cannot diffuse through the clay layer to the substrate electrode.

ACKNOWLEDGEMENTS

The support of the National Science Foundation (CHE8304666) and the Robert A. Welch Foundation (F-079) are gratefully acknowledged.

REFERENCES

1 (a) T.P. Henning, H.S. White and A.J. Bard, J. Am. Chem. Soc., 103 (1981) 3937; (b) T.P. Henning, H.S. White and A.J. Bard, ibid., 104 (1982) 5862; (c) T.P. Henning and A.J. Bard, J. Electrochem. Soc., 130 (1983) 613.
2 J.M. Thomas in M.A. Whittingham and A.J. Jacobson (Eds.), Intercalation Chemistry, Academic Press, New York, 1982, Ch. 3.
3 (a) R.M. Barrer, Zeolites and Clay Minerals as Sorbents and Molecular Sieves, Academic Press, London, 1978, Ch. 3; (b) B.K.G. Theng, The Chemistry of Clay-Organic Reactions, Wiley, New York, 1974.
4 (a) A. Shimoyama and W.D. Johns, Nature Phys. Sci., 232 (1971) 140; (b) B. Durand, R. Pelet and J.J. Fripat, Clays Clay Miner., 20 (1972) 21; (c) N. Oyama and F.C. Anson, J. Electroanal. Chem., 199 (1986) 467.
5 (a) H. Nijs, M. Cruz, J.J. Fripiat and H. Van Damme, J. Chem. Soc. Chem. Commun., (1981) 1026; (b) H. Nijs, J.J. Fripiat and H. Van Damme, J. Phys. Chem., 87 (1983) 1279; (c) F.-R.F. Fan, H.-Y. Liu and A.J. Bard, ibid., 89 (1985) 4418; (d) O. Enea and A.J. Bard, ibid., 90 (1986) 301; (e) S.L. Suib and K.A. Carrado, Inorg. Chem., 24 (1985) 863; (f) P.K. Ghosh, A.W.-H. Mau and A.J. Bard, J. Electroanal. Chem., 169 (1984) 315.
6 (a) T.J. Pinnavaia, Science, 220 (1983) 365; (b) T.J. Pinnavaia, M.-S. Tzou and S.D. Landau, J. Am. Chem. Soc., 107 (1985) 4783.
7 (a) E.T. Degens, J. Matheja and T.A. Jackson, Nature (London), 227 (1970) 492; (b) M. Paecht-Horowitz, J. Berger and A. Katchalsky, ibid., 228 (1970) 636; (c) M. Paecht-Horowitz, Angew. Chem. (Int. Ed. Engl.), 12 (1973) 349; (d) N. Lahav, D. White and S. Chang, Science, 201 (1978) 67; (e) S.C. Bondy and M.E. Harrington, ibid., 203 (1979) 1243.
8 (a) A. Yamagishi, J. Phys. Chem., 86 (1982) 2472; (b) A. Yamagishi, J. Chem. Soc. Chem. Commun., (1984) 119.
9 See, for example, (a) J. Zak and T. Kuwana, J. Am. Chem. Soc., 104 (1982) 5514; (b) C.G. Murray, R.J. Nowak and D.R. Rolison, J. Electroanal. Chem., 164 (1984) 205; (c) B. De Vismes, F. Bedioui, J. Devynck and C. Bied-Charreton, ibid., 187 (1985) 197.
10 See, for example, (a) D. Ellis, M. Eckhoff and V.D. Neff, J. Phys. Chem., 85 (1981) 1225; (b) K. Itaya, T. Ataka and S. Toshima, J. Am. Chem. Soc., 104 (1982) 4767; (c) K. Itaya, I. Uchida, S. Toshima and R.M. De La Rue, J. Electrochem. Soc., 131 (1984) 2086.
11 (a) F.-R.F. Fan and A.J. Bard, J. Electrochem. Soc., 133 (1986) 301; (b) C.M. Castro-Acuña, F.-R.F. Fan and A.J. Bard, unpublished experiments.
12 H. Van Olphen, An Introduction to Clay Colloid Chemistry, 2nd ed., Wiley, New York, 1977, (a) Ch. 5; (b) Ch. 2.
13 H. Van Olphen and J.J. Fripiat (Eds.), Data Handbook for Clay Materials and Other Nonmetallic Minerals, Pergamon Press, Oxford, 1979.
14 (a) E.M. Engler, Chem. Tech., (1976) 274; (b) J.H. Perlstein, Angew. Chem. (Int. Ed. Engl.), 16 (1977) 519; (c) A.F. Garito and A.J. Heeger, Acc. Chem. Res., 7 (1974) 232; (d) J.B. Torrance, ibid., 12 (1979) 79; (e) F. Wudl, ibid., 17 (1984) 227.
15 D. Ege, P.K. Ghosh, J.R. White, J.-F. Equey and A.J. Bard, J. Am. Chem. Soc., 107 (1985) 5644.
16 K. Itaya and A.J. Bard, J. Phys. Chem., 89 (1985) 5565.
17 A.J. Bard and L.R. Faulkner, Electrochemical Methods, Wiley, New York, 1982, (a) Ch. 4; (b) p. 218.
18 A.T. Hubbard and F.C. Anson in A.J. Bard (Ed.), Electroanalytical Chemistry, Vol. 4, Marcel Dekker, New York, 1970, pp. 129–214.

19 R.W. Murray in A.J. Bard (Ed.), Electroanalytical Chemistry, Vol. 13, Marcel Dekker, New York, 1982, pp. 191–368.
20 M. Majda and L.R. Faulkner, J. Electroanal. Chem., 169 (1984) 77.
21 R. Naegeli, J. Redepenning and F.C. Anson, J. Phys. Chem., 90 (1986) 6227.
22 (a) D.L. Coffen, J.Q. Chambers, D.R. Williams, P.E. Garret and N.D. Canfield, J. Am. Chem. Soc., 93 (1971) 2258; (b) J.B. Torrance, B.A. Scott, B. Welber, F.B. Kaufman and P.E. Seiden, Phys. Rev. B, 19 (1979) 730; (c) F. Wudl, G.M. Smith and E.J. Hufnagel, J. Chem. Soc. Chem. Commun., (1970) 1453; (d) M.R. Suchanski and R.P. Van Duyne, J. Electrochem. Soc., 123 (1976) 181c.
23 R.A. Schoonheydt in J.J. Fripiat (Ed.), Advanced Techniques for Clay Mineral Analysis, Elsevier, Amsterdam, 1982, Ch. 7.
24 M.T. Carter and A.J. Bard, unpublished results.
25 (a) J.R. White and A.J. Bard, unpublished results; (b) K. Bergmann and C.T. O'Konski, J. Phys. Chem., 67 (1963) 2169; (c) P.T. Hang and G.W. Brindley, Clays Clay Miner., 18 (1970) 203.
26 P.K. Ghosh and A.J. Bard, J. Am. Chem. Soc., 105 (1983) 5691.
27 H. Van Damme, F. Obrecht and M. Letellier, Nouv. J. Chim., 8 (1984) 681.
28 P.G. Slade and M. Raupach, Clays Clay Miner., 30 (1982) 297.
29 (a) F.B. Kaufman, E.M. Engler, D.C. Green and J.Q. Chambers, J. Am. Chem. Soc., 98 (1987) 1596; (b) K.-N. Kuo, P.R. Moses, J.R. Lenhard, D.C. Green and R.W. Murray, Anal. Chem., 51 (1979) 745; (c) J.Q. Chambers, D.C. Green, F.B. Kaufman, E.M. Engler, B.A. Scott and R.R. Schumaker, ibid., 49 (1977) 802.
30 H.-Y. Liu and F.C. Anson, J. Electroanal. Chem., 184 (1985) 411.
31 J.R. White and A.J. Bard, J. Electroanal. Chem., 197 (1986) 233.
32 (a) D.J. Greenland and J.P. Quirke, Clays Clay Miner., 9 (1962) 484; (b) P. Franzen, Clay Miner. Bull., 2 (1954) 223; (c) M.F. Traynor, M.M. Mortland and T.J. Pinnavaia, Clays Clay Miner., 26 (1978) 318.
33 P.J. Peerce and A.J. Bard, J. Electroanal. Chem., 114 (1980) 89 and references therein.
34 A.T. Hubbard, CRC Crit. Rev. Anal. Chem., 2 (1973) 201.
35 C.R. Martin, I. Rubinstein and A.J. Bard, J. Am. Chem. Soc., 104 (1982) 4817.
36 I. Rubinstein and A.J. Bard, J. Am. Chem. Soc., 103 (1981) 5007.
37 H. Angerstein-Kozlowska, J. Klinger and B.E. Conway, J. Electroanal. Chem., 75 (1977) 61.
38 (a) H. Angerstein-Kozlowska, J. Klinger and B.E. Conway, J. Electroanal. Chem., 75 (1977) 45; (b) E. Laviron, ibid., 122 (1981) 37.
39 E. Laviron, J. Electroanal. Chem., (a) 35 (1972) 333; (b) 39 (1972) 1.
40 F.B. Kaufman, A.H. Schroeder, E.M. Engler, S.R. Cramer and J.Q. Chambers, J. Am. Chem. Soc., 102 (1980) 483.
41 B.A.G. Knight and T.E. Tomlinson, J. Soil Sci., 18 (1967) 233.
42 B.K.G. Theng, Clays Clay Miner., 19 (1971) 383.
43 W.E. Rudzinski and A.J. Bard, J. Electroanal. Chem., 199 (1986) 323.
44 (a) M. Lamache, H. Menet and A. Moradpour, J. Am. Chem. Soc., 104 (1982) 4520; (b) C.D. Jaeger and A.J. Bard, ibid., 101 (1979) 1690; (c) C.D. Jaeger and A.J. Bard, ibid., 102 (1980) 5435.
45 (a) S.J. LaPlaca, P.W.R. Corfield, R. Thomas and B.A. Scott, Solid State Commun., 17 (1975) 635; (b) B.A. Scott, S.J. LaPlaca, J.B. Torrance, B.D. Silverman and B. Welber, J. Am. Chem. Soc., 99 (1977) 6631; (c) J.B. Torrance and B.D. Silverman, Phys. Rev. B, 15 (1977) 788; (d) R.J. Warmack and T.A. Callcott, ibid., 12 (1975) 3336.
46 D.J. Cebula, R.K. Thomas, S. Middleton, R.H. Ottewill and J.W. White, Clays Clay Miner., 27 (1979) 39.
47 T. Sudo, S. Shimoda, H. Yotsumoto and S. Aita, Electron Micrographs of Clay Minerals, Elsevier, Amsterdam, 1981, Ch. 1.